

Lawrence Berkeley National Laboratory

Recent Work

Title

PERTURBATIVE ANALYSIS OF THE QCD4 MAPS

Permalink

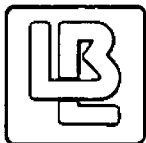
<https://escholarship.org/uc/item/3dm8s73f>

Authors

Bern, Z.
Chan, H.S.

Publication Date

1985



Lawrence Berkeley Laboratory

UNIVERSITY OF CALIFORNIA

Physics Division

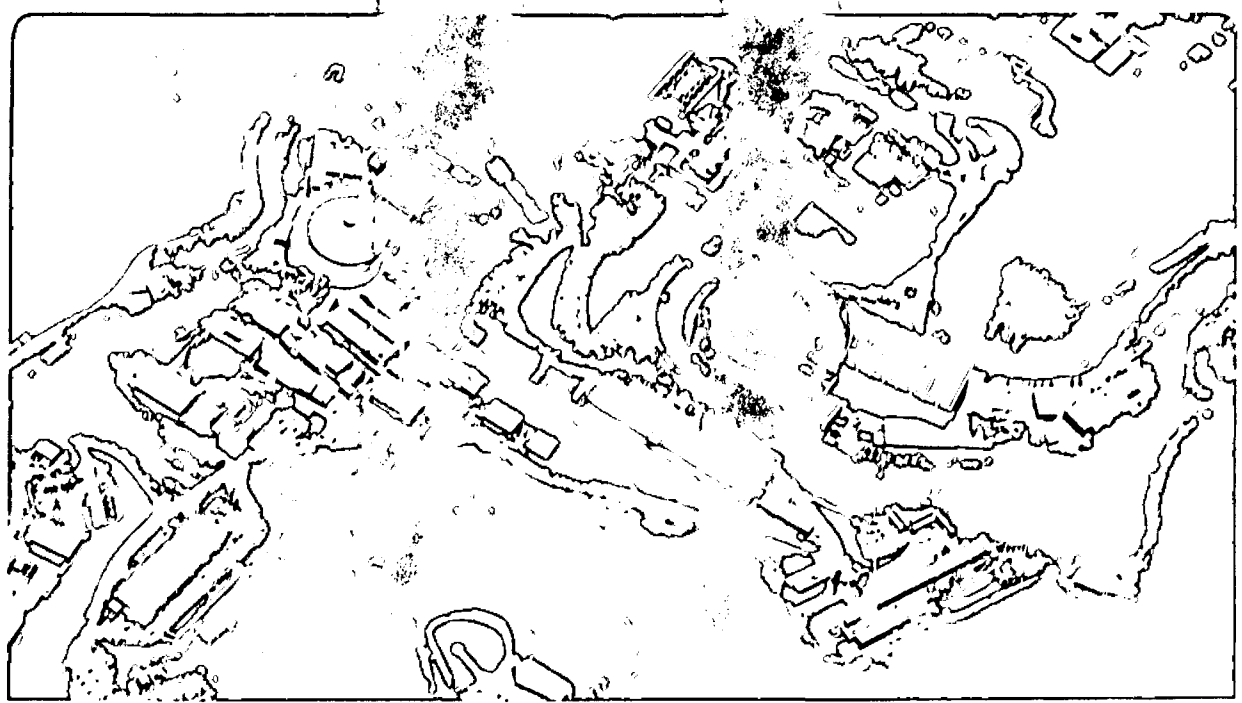
RECEIVED
LAWRENCE
BERKELEY LABORATORY
MAR 26 1985
LIBRARY AND
DOCUMENTS SECTION

Submitted for publication

PERTURBATIVE ANALYSIS OF THE QCD₄ MAPS

Z. Bern and H.S. Chan

January 1985



LBL-19001
c.2

DISCLAIMER

This document was prepared as an account of work sponsored by the United States Government. While this document is believed to contain correct information, neither the United States Government nor any agency thereof, nor the Regents of the University of California, nor any of their employees, makes any warranty, express or implied, or assumes any legal responsibility for the accuracy, completeness, or usefulness of any information, apparatus, product, or process disclosed, or represents that its use would not infringe privately owned rights. Reference herein to any specific commercial product, process, or service by its trade name, trademark, manufacturer, or otherwise, does not necessarily constitute or imply its endorsement, recommendation, or favoring by the United States Government or any agency thereof, or the Regents of the University of California. The views and opinions of authors expressed herein do not necessarily state or reflect those of the United States Government or any agency thereof or the Regents of the University of California.

January 1985

LBL-19001

**PERTURBATIVE ANALYSIS
OF
THE QCD₄ MAPS¹**

Zvi Bern

and

Hue Sun Chan

**Lawrence Berkeley Laboratory
University of California
Berkeley, California 94720**

ABSTRACT

The Claudson-Halpern stochastic processes for QCD₄ are verified to all orders of perturbation theory resulting in a number of new finite-time, infrared finite, perturbation expansions of the theory. The map viewpoint shows that the superficial quadratic divergences of QCD₄, at least in the temporal gauge, are related to the choice of any particular final state configuration in the Feynman path integral formulation.

¹This work was supported by the Director, Office of Energy Research, Office of High Energy and Nuclear Physics, Division of High Energy Physics of the US Department of Energy under contract DE-AC03-76SF00098.

1. Introduction

Recently, Claudson and Halpern [1, 2] constructed a pair of Nicolai maps [3], or stochastic processes [4] for ordinary non-supersymmetric pure Yang-Mills in four dimensions. The maps describe QCD_4 as a nonequilibrating brownian motion in real (euclidean) time, and have constant Jacobians, so no fermions are needed for any cancellation. Only very few ordinary bosonic theories can have such closed form maps [2], and QCD_4 is singled out in this respect. The possibility of such mappings is directly traceable to the existence of the Loos-Greensite [5] zero-energy winding number solutions.

The perturbative equivalence of the maps to the conventional formulation is by no means obvious, since, for example, each map is an apparently parity-violating formulation of the theory. The major goal of this paper is to show the complete perturbative equivalence of the map formulation to the conventional functional integral formulation. In this we are successful, generating in the process a number of new perturbation expansions of QCD_4 in the temporal gauge, with boundary conditions at finite times. The expansions may be useful, because at finite-time the temporal gauge is infrared finite.

Additionally, we had the following motivation: In the map language, the gauge field is solved iteratively in terms of a random noise field, η , and diagrams that represent correlation functions are formed by η -contractions of these solutions in a way analogous to that of Parisi and Wu's fifth-time stochastic quantization [6]. By a naive power count, based on imposing well behaved boundary conditions that prevent the runaway, instead of the required retarded boundary conditions, the Claudson-Halpern maps are such that the pure map diagrams appear linearly divergent at worst. This offers a hope that the superficial quadratic divergences of QCD_4 could be avoided. However, in the Claudson and Halpern construction, the boundary conditions are retarded and there is a final state constraint. As we shall see, it is this final state constraint that reintroduces the superficial quadratic divergences. Since the map formulation is equivalent to QCD_4 , the final state constraint is nothing more than a choice of any particular final state in the Feynman functional integral formulation. Curiously, both a choice of final state and the superficial quadratic divergences are apparent breakdowns of gauge invariance. Connected with this, we find that the stochastic regular-

ization proposed by Claudson and Halpern fails precisely because it does not regularize the choice of the final state.

The organization of this paper is as follows. Section 2 is an overview of the QCD₄ Nicolai maps. Diagrammatic expansion rules for the maps, as well as an explicit one loop example of the rules are given in section 3. In section 4, the map diagrams are organized into a new set of diagrams which we call first order diagrams, since they correspond to a first order formalism of QCD₄. In section 5, these first order diagrams are further reorganized into the finite-time Feynman diagrams of QCD₄. Section 6 contains a discussion of the role of the initial and final configurations. The conclusions and comments are given in section 7.

2. Overview of Nicolai maps in QCD₄

Claudson and Halpern formally established the identity,

$$\begin{aligned} \langle F_i^a | \exp(-\hat{H}T) | I_i^a \rangle &= \int_{A_i^a(t_1)=I_i^a}^{A_i^a(t_2)=F_i^a} \mathcal{D}A_i^a e^{-S_{QCD}} \\ &= e^{\pm(W[F]-W[I])} \langle e^{\pm\xi[A^\pm]} \delta[A_i^{\alpha\pm}(t_2) - F_i^a] \rangle_\eta \end{aligned} \quad (2.1)$$

where $T = t_2 - t_1$ and \hat{H} is the QCD₄ Hamiltonian. $I_i^a(\vec{x})$ and $F_i^a(\vec{x})$ are respectively the initial and final configurations of A_i^a at t_1 and t_2 . In identity (2.1), W and ξ are related to the winding number current. For our purpose of perturbative calculation, we can make the standard assumption that total divergences integrate to zero, and therefore $\xi[A]$ can be ignored [1]. S_{QCD} is the usual euclidean QCD₄ action in the temporal gauge,

$$S_{QCD} = \frac{1}{2} \int_{t_1}^{t_2} dt \int d^3x [E_i^a E_i^a + B_i^a B_i^a], \quad (2.2)$$

and the η -average is performed with the gaussian Boltzman factor,

$$e^{-\frac{1}{2} \int_{t_1}^{t_2} dt \int d^3x \eta_i^a(\vec{x},t) \eta_i^a(\vec{x},t)}, \quad (2.3)$$

using either of the pair of Langevin-Nicolai maps discovered by Claudson and Halpern,

$$E_i^{\alpha\pm} = \mp B_i^{\alpha\pm} + \eta_i^a, \quad (2.4)$$

in which,

$$E_i^a = \dot{A}_i^a, \quad B_i^a = \frac{1}{2} \epsilon_{ijk} F_{jk}^a, \quad F_{jk}^a = \partial_j A_k^a - \partial_k A_j^a - gf^{abc} A_j^b A_k^c. \quad (2.5)$$

This Langevin equation (2.4) is a stochastic differential equation [4] driven by the random noise field η_i^a . The maps must be started at the initial condition of the transition amplitude $I_i^a(\vec{x})$, and the δ -functional in eq. (2.1) (final state constraint) picks out only those brownian motions that end at the final state specified in the transition amplitude. QCD₄ is thus described as a brownian motion from I to F , as illustrated in fig. 2-1.

The finite-time expectation values of an arbitrary functional $G[A]$ can be expressed simply in terms of averages over the η field. Namely,

$$\langle G[A] \rangle \equiv \frac{\int_{A_i^a(t_1)=I_i^a}^{A_i^a(t_2)=F_i^a} \mathcal{D}A_i^a G[A] e^{-S_{QCD}[A]}}{\int_{A_i^a(t_1)=I_i^a}^{A_i^a(t_2)=F_i^a} \mathcal{D}A_i^a e^{-S_{QCD}[A]}} \quad (2.6)$$

$$= \frac{\langle \delta[A_i^{a\pm}(t_2) - F_i^a] G[A^\pm] \rangle_\eta}{\langle \delta[A_i^{a\pm}(t_2) - F_i^a] \rangle_\eta}. \quad (2.7)$$

Note that the $\exp(\pm W)$ factors do not contribute to this average, because of cancellation between the numerator and denominator.

In order to compute these η averages, the gauge field A has to be solved as a functional of the η noise field, through the map equations (2.4). The maps are equivalent to the integral equations,

$$A_i^{a\pm}(\vec{x}, t) = \left(e^{\mp(t-t_1)D} \right)_{ik} I_k^a(\vec{x}) + \int_{t_1}^t d\tau \left(e^{\mp(t-\tau)D} \right)_{ik} \left\{ \eta_k^a \pm \frac{1}{2} g \epsilon_{klm} f^{abc} A_l^{b\pm}(\vec{x}, \tau) A_m^c(\vec{x}, \tau) \right\}, \quad (2.8)$$

where $D_{ij} = -\epsilon_{ijk} \partial_k$. These integral equations explicitly contain the retarded Langevin boundary conditions (causality) necessary to prevent the introduction of spurious fermions, as well as the initial condition, $A_i^{a\pm}(\vec{x}, t_1) = I_i^a(\vec{x})$. The retarded Green function of the Langevin equations are

$$G_{ij}^\pm(\vec{x} - \vec{x}', t - t') = \theta(t - t') \left(e^{\mp(t-t')D} \right)_{ij} \delta^3(\vec{x} - \vec{x}') \quad (2.9)$$

$$= \theta(t - t') \left(\hat{L}_{ij} + \hat{T}_{ij}^+ e^{\mp(t-t')\sqrt{-\nabla^2}} + \hat{T}_{ij}^- e^{\pm(t-t')\sqrt{-\nabla^2}} \right) \delta^3(\vec{x} - \vec{x}'), \quad (2.10)$$

where \hat{L}_{ij} and \hat{T}_{ij} are respectively the standard longitudinal and transverse projection operators, while \hat{T}_{ij}^\pm are the transverse helicity projection operators defined by

$$\hat{T}_{ij}^\pm = \frac{1}{2} \left(\hat{T}_{ij} \pm \frac{D_{ij}}{\sqrt{-\nabla^2}} \right). \quad (2.11)$$

As in Parisi and Wu's fifth-time stochastic quantization of gauge fields [6], there is no damping in the longitudinal mode of the Langevin Green function. However, in this case there is also an exponential runaway in the transverse mode associated with the nonequilibrating nature of the QCD₄ maps.

Conventionally, one believes that the precise value of the initial and final conditions should be irrelevant in perturbation theory at large times, T , so in the first stage of the computation we shall simply assume $I = F = 0$. The effect of $I, F \neq 0$ in perturbation theory will be discussed in section 6.

The integral equations (2.8) can be solved iteratively by

$$A_i^{\alpha\pm} = A_i^{\alpha\pm(0)} + gA_i^{\alpha\pm(1)} + g^2A_i^{\alpha\pm(2)} + \dots, \quad (2.12)$$

where

$$A_i^{\alpha\pm(0)}(\vec{x}, t) = \int_{t_1}^t d\tau \left(e^{\mp(t-\tau)D} \right)_{ij} \eta_j^\alpha(\vec{x}, \tau), \quad (2.13)$$

$$gA_i^{\alpha\pm(1)}(\vec{x}, t) = \pm \frac{1}{2} g \epsilon_{klm} f^{abc} \int_{t_1}^t d\tau \left(e^{\mp(t-\tau)D} \right)_{ik} A_l^{b\pm(0)}(\vec{x}, \tau) A_m^{c\pm(0)}(\vec{x}, \tau), \quad (2.14)$$

$$g^2A_i^{\alpha\pm(2)}(\vec{x}, t) = \pm g^2 \epsilon_{klm} f^{abc} \int_{t_1}^t d\tau \left(e^{\mp(t-\tau)D} \right)_{ik} A_l^{b\pm(1)}(\vec{x}, \tau) A_m^{c\pm(0)}(\vec{x}, \tau). \quad (2.15)$$

These iterative solutions are represented diagrammatically as tree diagrams in fig. 2-2, where arrowed lines represent the Langevin Green function (2.9) and the crosses stand for the η noise field. Note that only cubic vertices are required in the maps, in distinction to Parisi and Wu's fifth-time formulation [6], in which quartic vertices are also present. If it were not for the necessity of expanding the final state constraint, the expectation values could easily be computed in the usual way, with gaussian η -contractions. In diagrammatic language this is achieved by gluing together the crosses of the tree diagrams. For example, the two point function through order g^2 could be given by the diagrams in fig. 2-3.

A naive power count, based on using well behaved instead of retarded boundary conditions, indicates that the two point functions of fig. 2-3 are not quadratically divergent, but linearly divergent at worst. This is because the cubic coupling involves no derivative, while the Langevin Green function

$$G_{ij}^\pm = (\partial_t \delta_{ij} \mp \epsilon_{ijk} \partial_k)^{-1} \sim \frac{1}{k}, \quad (2.16)$$

where k is either a power of momentum or energy. In fact, it is misleading to simply assign $1/k$ to each Green function in the two point correlation (fig. 2-3). This is because the well behaved boundary conditions ignore

the nonequilibration or runaway that occurs, in the maps, with the required retarded boundary conditions. The diagrams have extra dimensionless loop divergences from the runaway term, e^{pT} , where p is the loop momentum. Still the argument is suggestive because, as we will see below, the final state constraint removes the extra e^{pT} divergences while introducing the superficial quadratic divergences.

3. Map Diagrams

The iterative expansion (2.12) of A in terms of η can be used to construct a new perturbative expansion of the Yang-Mills Green functions. In sections 4 and 5 the complete equivalence of this new expansion to the standard perturbative expansion will be shown. A systematic way of perturbatively expanding the expectation values (2.6) is by making use of the map generating functional

$$\begin{aligned}
Z^m[J] &\equiv \frac{\langle \delta[A_i^{\alpha\pm}(t_2)] \exp\left(\int_{t_1}^{t_2} dt \int d^3x J_i^\alpha A_i^{\alpha\pm}\right) \rangle_\eta}{\langle \delta[A_i^{\alpha\pm}(t_2)] \rangle_\eta} \\
&= \int \mathcal{D}\eta \mathcal{D}\lambda \exp \left[\int_{t_1}^{t_2} dt \int d^3x \left(-\frac{1}{2} \eta_i^\alpha(\vec{x}, t) \eta_i^\alpha(\vec{x}, t) + J_i^\alpha(\vec{x}, t) A_i^{\alpha\pm}(\vec{x}, t) \right) \right. \\
&\quad \left. + i \int d^3x \lambda_i^\alpha(\vec{x}) A_i^{\alpha\pm}(\vec{x}, t_2) \right] \\
&\quad \times \left\{ \int \mathcal{D}\eta \mathcal{D}\lambda \exp \left[- \int_{t_1}^{t_2} dt \int d^3x \frac{1}{2} \eta_i^\alpha(\vec{x}, t) \eta_i^\alpha(\vec{x}, t) \right. \right. \\
&\quad \left. \left. + i \int d^3x \lambda_i^\alpha(\vec{x}) A_i^{\alpha\pm}(\vec{x}, t_2) \right] \right\}^{-1}, \tag{3.1}
\end{aligned}$$

where the standard Fourier representation of the final state constraint has been used. Note that the constraint field $\lambda_i^\alpha(\vec{x})$ is a function of only the three spatial dimensions and F_i^α is taken to vanish.

The perturbative calculation of this generating functional (3.1) is slightly different than usual calculations in quantum field theory. Usually the nontrivial interactions are contained in the action; however, in this case the "action", $\frac{1}{2}\eta^2$, is trivial, while the interactions are contained in the nontrivial nature of A as a functional of η . There are two contributions to the perturbative expansion of the generating functional (3.1). One contribution is from the coupling of the gauge field to the external source, J , while the other is from the final state constraint. The perturbative expansion is carried out by substituting the Langevin expansion (2.12) into the generating functional, $Z^m[J]$. It is convenient to introduce an additional external source,

$\zeta_i^a(\vec{x})$, in the zeroth order generating functional, to be used in the perturbative expansion of the final state constraint. Using the fact that the n -th order gauge field, $A^{(n)}[A^{(0)}; \vec{x}, t]$, can be written as a functional of $A^{(0)}(\vec{x}, t)$, as in eq. (2.15), the generating functional (3.1) can be rewritten as:

$$Z^m[J] = N \exp \left\{ \int_{t_1}^{t_2} dt \int d^3x J_i^a(\vec{x}, t) \sum_{n=1}^{\infty} g^n A_i^{a\pm(n)} \left[\frac{\delta}{\delta J}; \vec{x}, t \right] \right. \\ \left. + i \int d^3x \frac{\delta}{\delta \zeta_i^a(\vec{x})} \sum_{n=1}^{\infty} g^n A_i^{a\pm(n)} \left[\frac{\delta}{\delta J}; \vec{x}, t_2 \right] \right\} Z_0^m[J, \zeta] \Big|_{\zeta=0} : \quad (3.2)$$

where

$$Z_0^m[J, \zeta] \equiv \frac{\langle \delta[A_i^{a\pm(0)}(t_2) - i\zeta_i^a] \exp \int_{t_1}^{t_2} dt \int d^3x J_i^a A_i^{a\pm(0)} \rangle_{\eta}}{\langle \delta[A_i^{a\pm(0)}(t_2)] \rangle_{\eta}} \\ = N' \int \mathcal{D}\eta \mathcal{D}\lambda \exp \left[\int_{t_1}^{t_2} dt \int d^3x \left(-\frac{1}{2} \eta_i^a(\vec{x}, t) \eta_i^a(\vec{x}, t) \right. \right. \\ \left. \left. + J_i^a(\vec{x}, t) A_i^{a\pm(0)}(\vec{x}, t) \right. \right. \\ \left. \left. + i \int d^3x \lambda_i^a(\vec{x}) \left(A_i^{a\pm(0)}(\vec{x}, t_2) - i\zeta_i^a(\vec{x}) \right) \right] \right]. \quad (3.3)$$

N is an appropriate normalization, so that $Z^m[0] = 1$. The exponential term in eq. (3.2) containing the derivative with respect to the constraint external source, $\zeta_i^a(\vec{x})$, generates the higher order corrections to the constraint. Diagrams containing contributions from this term we call constraint diagrams. Diagrams which do not contain the higher order constraint contributions we call basic diagrams. Note that basic diagrams implicitly contain the zeroth order constraint contribution.

Since eq. (2.12) gives $A^{(0)\pm}$ linearly in terms of η , $Z_0^m[J, \zeta]$ can be obtained by Gaussian integration. Namely,

$$Z_0^m[J, \zeta] = \exp \left[\frac{1}{2} \int d^3x d^3x' \int_{t_1}^{t_2} dt dt' J_i^a(\vec{x}, t) \Delta_{ij}^{AA}(\vec{x}, t; \vec{x}', t') J_j^a(\vec{x}', t') \right. \\ \left. + i \int d^3x d^3x' \int_{t_1}^{t_2} dt J_i^a(\vec{x}, t) \Delta_{ij}^{A\lambda}(\vec{x}, t; \vec{x}') \zeta_j^a(\vec{x}') \right. \\ \left. + \frac{1}{2} \int d^3x d^3x' \zeta_i^a(\vec{x}) \Delta_{ij}^{\lambda\lambda}(\vec{x}; \vec{x}') \zeta_j^a(\vec{x}') \right], \quad (3.4)$$

where

$$\begin{aligned} \Delta_{ij}^{AA}(\vec{x}, t; \vec{x}', t') &= \left[\left\{ \frac{1}{T} \theta(t' - t) (t - t_1)(t_2 - t') + (t \leftrightarrow t') \right\} \hat{L}_{ij} \right. \\ &\quad + \left\{ \theta(t' - t) \frac{\sinh[(t_2 - t')\sqrt{-\nabla^2}] \sinh[(t - t_1)\sqrt{-\nabla^2}]}{\sqrt{-\nabla^2} \sinh[T\sqrt{-\nabla^2}]} \right. \\ &\quad \left. \left. + (t \leftrightarrow t') \right\} \hat{T}_{ij} \right] \delta^3(\vec{x} - \vec{x}'), \end{aligned} \quad (3.5a)$$

$$\Delta_{ij}^{A\lambda}(\vec{x}, t; \vec{x}') = \left[\frac{t - t_1}{T} \hat{L}_{ij} + \frac{\sinh[(t - t_1)\sqrt{-\nabla^2}]}{\sinh[T\sqrt{-\nabla^2}]} \hat{T}_{ij} \right] \delta^3(\vec{x} - \vec{x}'), \quad (3.5b)$$

$$\Delta_{ij}^{\lambda\lambda}(\vec{x}, \vec{x}') = \left[\frac{1}{T} \hat{L}_{ij} + \frac{\sqrt{-\nabla^2} e^{\pm T\sqrt{-\nabla^2}}}{\sinh[T\sqrt{-\nabla^2}]} \hat{T}_{ij}^{\pm} + \frac{\sqrt{-\nabla^2} e^{\mp T\sqrt{-\nabla^2}}}{\sinh[T\sqrt{-\nabla^2}]} \hat{T}_{ij}^{\mp} \right] \delta^3(\vec{x} - \vec{x}'). \quad (3.5c)$$

As defined previously, $T = t_2 - t_1$, while \hat{L}_{ij} , \hat{T}_{ij} , and \hat{T}_{ij}^{\pm} are the projection operators.

A systematic way of generating all A-field correlation functions is summarized by the following diagrammatic rules in (t, \vec{p}) space, where (t, \vec{p}) stands for coordinate (euclidean) time and spatial momentum. In Parisi and Wu's fifth-time formulation two types of propagators were needed; however, in our case, two extra propagators arise from the final state constraint. The four propagators are:

$$\begin{aligned} i^a \xrightarrow{p} j^b &\equiv \delta^{ab} G_{ij}^{\pm}(p, t - t') \\ &\equiv \delta^{ab} \theta(t - t') \left[\hat{L}_{ij} + e^{\mp(t-t')p} \hat{T}_{ij}^+ + e^{\pm(t-t')p} \hat{T}_{ij}^- \right]. \end{aligned} \quad (3.6)$$

The above propagator is the usual retarded Green function of the Langevin equation (2.4), in momentum space. As in Parisi and Wu's fifth-time stochastic quantization, the directionality of the Langevin Green function follows from the causality imposed on the Langevin equation. However, as mentioned previously, these Green functions differ from the Parisi and Wu Green functions in that one helicity becomes unbounded for large $t - t'$.

$$\begin{aligned} i^a \overset{p}{\rightsquigarrow} j^b &\equiv \delta^{ab} \Delta_{ij}^{AA}(p, t', t) = \delta^{ab} \Delta_{ij}^{AA}(p, t, t') \\ &\equiv \delta^{ab} \left[\frac{1}{T} \theta(t' - t) (t - t_1)(t_2 - t') \hat{L}_{ij} \right. \\ &\quad \left. + \theta(t' - t) \frac{\sinh[(t_2 - t')p] \sinh[(t - t_1)p]}{p \sinh[Tp]} \hat{T}_{ij} + (t \leftrightarrow t') \right]. \end{aligned} \quad (3.7)$$

Although the propagator (3.7) is related to the pure map zeroth order two point function ($\leftarrow \times \rightarrow$) (fig. 2-3), it contains an extra contribution from

the zeroth order final state constraint, which prevents the runaway behavior.

$$\begin{aligned}
i \overset{a}{\text{---}} \overset{p}{\text{---}} \overset{b}{\text{---}} j t_2 &\equiv \delta^{ab} \Delta_{ij}^{A\lambda}(p, t) \\
&\equiv \delta^{ab} \left[\frac{t-t_1}{T} \hat{L}_{ij} + \frac{\sinh[(t-t_1)p]}{\sinh[Tp]} \hat{T}_{ij} \right].
\end{aligned} \tag{3.8}$$

Propagator (3.8) represents a mixing between the physical gauge field, $A_i^a(\vec{x}, t)$, and the constraint field, $\lambda_i^a(\vec{x})$, which exists only at t_2 .

$$\begin{aligned}
i \overset{a}{\text{---}} \overset{p}{\text{---}} \overset{b}{\text{---}} j t_2 &\equiv \delta^{ab} \Delta_{ij}^{\lambda\lambda}(p) \\
&\equiv \delta^{ab} \left[\frac{1}{T} \hat{L}_{ij} + \frac{pe^{\pm Tp}}{\sinh[Tp]} \hat{T}_{ij}^+ + \frac{pe^{\mp Tp}}{\sinh[Tp]} \hat{T}_{ij}^- \right].
\end{aligned} \tag{3.9}$$

This is the propagator of the constraint field. Both ends must join to t_2 points. Actually the propagators (3.7), (3.8) and (3.9) are the spatial Fourier transforms of the propagators defined in eq. (3.5). The last two propagators involving t_2 come explicitly from the final state constraint.

Since $A^{(n)}[A^{(0)}; \vec{x}, t]$ contains $n+1$ factors of $A^{(0)}$ it may seem that the map generating functional (3.2) contains an infinite number of different vertices. However, $A^{(n)}[A^{(0)}; \vec{x}, t]$ is a nonlocal functional of $A^{(0)}$, because $A^{(n)}$ is related to $A^{(0)}$ through the Langevin Green functions, G^\pm , as given, for example, in eq. (2.15). These nonlocal vertex factors can be rearranged into five local vertex factors (fig 3-1). Each three-point vertex connects to at least one G^\pm propagator. As with usual Feynman diagrams three-momenta are conserved at vertices, all internal momenta are integrated, intermediate times are integrated from t_1 to t_2 , and combinatoric factors are included in the usual fashion. If there are any G^\pm propagators that join to external points, the rule is that the directions of the arrows (time) are always towards the external point, analogous to Parisi and Wu's stochastic quantization.

As an explicit example to illustrate these rules, we shall exhibit the order g^2 diagrams of the two-point correlation function,

$$N \int d^3x e^{-i\vec{p}\cdot\vec{x}} \left\langle A_i^{a\pm}(\vec{x}, t) A_j^{b\pm}(\vec{0}, t') \delta[A_i^{a\pm}(t_2)] \right\rangle_\eta. \tag{3.10}$$

The diagrams are divided into two classes. The basic diagrams are those that do not involve any t_2 vertices (or dotted propagators), while the constraint diagrams are those that contain at least one t_2 vertex, which occurs only in higher order terms in the expansion of the final state constraint. All the order g^2 diagrams are shown in fig. 3-2.

As we shall explain in the next section, the remaining runaway behavior caused by the G^\pm propagators is, in fact, fictitious and can be removed by

appropriately combining propagators. On the other hand, the superficial quadratic divergences are real, and are contained solely in the constraint diagrams (d) and (h) of fig. 3-2. This is precisely the reason for the failure of Claudson and Halpern's [1] proposed stochastic regularization scheme. Their scheme does not regularize the constraint propagators (3.8) and (3.9).

4. First order formalism diagrams

The map diagrams of the last section are quite complicated. However, the number of diagrams can be drastically reduced by making use of two new propagators defined as

$$\begin{aligned}
\Delta_{ij}^{\pi A \pm}(p, t', t) &\equiv G_{ij}^{\pm}(p, t - t') - G_{ik}^{\pm}(p, t_2 - t') \Delta_{kj}^{\lambda \lambda}(p, t) \\
&= \hat{L}_{ij} \left[\theta(t - t') - \frac{t - t_1}{T} \right] \\
&\quad + \hat{T}_{ij}^+ \left[\theta(t - t') e^{\mp(t-t')p} + \frac{e^{\mp(2T+t-t')p} - e^{\mp(2t_2-t-t')p}}{1 - e^{\mp 2Tp}} \right] \\
&\quad + \hat{T}_{ij}^- \left[\theta(t - t') e^{\pm(t-t')p} + \frac{e^{\pm(2T+t-t')p} - e^{\pm(2t_2-t-t')p}}{1 - e^{\pm 2Tp}} \right],
\end{aligned} \tag{4.1}$$

and

$$\begin{aligned}
\Delta_{ij}^{\pi \pi \pm}(p, t', t) &\equiv -G_{ik}^{\pm}(p, t_2 - t') \Delta_{kl}^{\lambda \lambda}(p) G_{lj}^{\pm}(p, t_2 - t) \\
&= - \left[\hat{L}_{ij} \frac{1}{T} \pm 2p \hat{T}_{ij}^+ \frac{e^{\mp(2t_2-t-t')p}}{1 - e^{\mp 2Tp}} \mp 2p \hat{T}_{ij}^- \frac{e^{\pm(2t_2-t-t')p}}{1 - e^{\pm 2Tp}} \right].
\end{aligned} \tag{4.2}$$

The superscripts, πA and $\pi \pi$, will be explained at the end of this section. For now, it is sufficient to know that these two new propagators are combinations of the map constraint propagators with the Langevin Green function. This is illustrated in fig. 4-1. Note that these new propagators do not contain any runaway behavior for $T \rightarrow \infty$, so diagrams constructed from these propagators will not contain the e^{pT} divergence of pure map diagrams (fig. 2-3). If these new propagators are used in place of the map propagators there is no need for the t_2 constraint vertices (fig. 3-1a, 3-1b) since these are absorbed into the definitions of the new propagators. The three cubic couplings in the maps (fig. 3-1c, 3-1d, 3-1e) can be rewritten as cubic vertices connecting the Δ_{ij}^{AA} , $\Delta_{ij}^{\pi A}$ and $\Delta_{ij}^{\pi \pi}$ propagators, as shown in fig. 4-2. In particular, the sixteen order g^2 map diagrams for the two-point function (fig. 3-2) are combined into five first order formulation diagrams (fig. 4-3).

We note that at infinite T only diagram (b) in fig. 4-3 is quadratically divergent. This is because the Δ_{ij}^{AA} propagator is $O(p^{-2})$ while the $\Delta_{ij}^{\pi A}$

propagator is $O(p^{-1})$. The $\Delta_{ij}^{\pi\pi}$ propagator vanishes in the infinite T limit. Instead of having the quadratic divergences distributed in two diagrams as in the usual formulation, this first order formulation has the virtue of isolating all the quadratic divergences of the order g^2 two-point function in one diagram. This makes it easier to deal with when analysis of the quadratic divergences is made.

The relationship between this formalism and the map formalism reveals the origin of the superficial quadratic divergence. The only quadratically divergent first order diagram (b) in fig. 4-3 is equivalent to the three map diagrams in fig. 4-4. These three map diagrams are constraint diagrams. That is, they contain higher order contributions of the perturbative expansion of the final state constraint on the maps. This confirms that the superficial quadratic divergences in the theory are related to a particular choice of final state.

On closer examination, we found that the diagrammatic rules given in this section correspond to the theory described by the first order generating functional

$$\begin{aligned} Z^\pi[J, K] &= N \int_{A_i^a(t_1)=0}^{A_i^a(t_2)=0} \mathcal{D}A_i^a \mathcal{D}\pi_j^b \exp \left[\int_{t_1}^{t_2} dt \int d^3x \left(-\frac{1}{2} \pi_i^a \pi_i^a \right. \right. \\ &\quad \left. \left. - i \pi_i^a (\dot{A}_i^a \pm \epsilon_{ijk} \partial_j A_k^a \mp \frac{1}{2} \epsilon_{ijk} f^{abc} A_j^b A_k^c) + J_i^a A_i^a + i K_i^a \pi_i^a \right) \right] \\ &= \exp \left[\pm \frac{1}{2} \int_{t_1}^{t_2} dt \int d^3x g f^{abc} \epsilon_{ijk} \frac{\delta}{\delta K_i^a} \frac{\delta}{\delta J_j^b} \frac{\delta}{\delta J_k^c} \right] Z_0^\pi[J, K], \end{aligned} \quad (4.3)$$

where

$$\begin{aligned} Z_0^\pi[J, K] &= N' \int_{A_i^a(t_1)=0}^{A_i^a(t_2)=0} \mathcal{D}A_i^a \mathcal{D}\pi_j^b \exp \left[\int_{t_1}^{t_2} dt \int d^3x \left(-\frac{1}{2} \pi_i^a \pi_i^a \right. \right. \\ &\quad \left. \left. - i \pi_i^a (\dot{A}_i^a \pm \epsilon_{ijk} \partial_j A_k^a) + J_i^a A_i^a + i K_i^a \pi_i^a \right) \right]. \end{aligned} \quad (4.4)$$

By gaussian integration, the A - A , π - A and π - π propagators are respectively found to be the functions Δ_{ij}^{AA} , $\Delta_{ij}^{\pi A}$ and $\Delta_{ij}^{\pi\pi}$ defined in eq. (3.5a), eq. (4.1) and eq. (4.2). We call the generating functional (4.3) a first order formulation of QCD₄. This first order formulation serves as an intermediate link between the map formulation and the usual path integral formulation of QCD₄. As mentioned previously, the importance of this formulation is that it reveals the connection between the final state constraint and the quadratic divergence. Also the one-loop superficial quadratic divergence of the theory is contained in a single diagram.

The next logical step is to show that the first order formalism diagrams are equivalent to the usual Feynman diagrams. Although this can be shown by a formal functional integration over the auxiliary field, π , this paper is concerned with making an explicit connection through perturbation theory. The perturbative connection will be accomplished in the next section.

5. Finite-time Feynman diagrams

In this section, our purpose is to reorganize the first order formalism diagrams of the last section into diagrams that contain only A - A propagators. As we shall see, the reorganized diagrams are just the finite-time Feynman diagrams of QCD_4 . To achieve this, two steps are needed: 1) Express the π - π and π - A propagators as combinations of A - A propagators and some appropriate factors to be determined. 2) Absorb these factors into the first order formalism vertices to turn them into standard QCD_4 three- and four-point vertices.

The first step is accomplished by noting two identities. First, the π - A propagator (4.1) can be expressed as

$$\Delta_{ij}^{\pi A \pm}(p, t', t) = \int_{t_1}^{t_2} dt'' \Theta_{ik}^{\pm}(p, t', t'') \Delta_{kj}^{AA}(p, t'', t), \quad (5.1)$$

where

$$\begin{aligned} \Theta_{ij}^{\pm}(p, t', t'') &= [\partial_\nu \hat{L}_{ij} + (\partial_\nu \pm p) \hat{T}_{ij}^+ + (\partial_\nu \mp p) \hat{T}_{ij}^-] \delta(t' - t'') \\ &= (\partial_\nu \delta_{ij} \pm i\epsilon_{ijk} p_k) \delta(t' - t''). \end{aligned} \quad (5.2)$$

As required, the π - A propagator is decomposed into a product of an A - A propagator and a Θ -factor as illustrated in fig. 5-1. The π - π propagator can also be rewritten in an analogous manner.

$$\begin{aligned} \Delta_{ij}^{\pi\pi \pm}(p, t', t) &= -\delta_{ij} \delta(t - t') \\ &+ \int_{t_1}^{t_2} d\tau \int_{t_1}^{t_2} ds \Theta_{ik}^{\pm}(p, t', \tau) \Delta_{ki}^{AA}(p, \tau, s) \Theta_{lj}^{\pm}(p, t, s). \end{aligned} \quad (5.3)$$

Now we proceed with the second step of absorbing these Θ -factors into vertex factors. Making use of the first identity (5.1), three possible permutations of the first order formalism vertices (fig. 4-2) combine to form a new three point vertex joining three A - A propagators (3.5a) together (fig. 5-2). Instead of a vertex for two A - and one π -field, the first order formalism vertex (fig. 5-2a) can be thought of as a vertex connecting three A -fields. By eq. (5.1), this new vertex factor is the product of a Θ -factor, $(\partial_\nu \delta_{ij} \pm i\epsilon_{ilm} p_m)$

and the first order formalism vertex factor, $\pm g f^{abc} \epsilon_{ijk}$. Adding this to the other two permutations, fig. 5-2 (b) and (c), gives

$$\pm g f^{abc} [\epsilon_{ijk} (\pm i \epsilon_{ilm} p_m) + \epsilon_{ilk} (\pm i \epsilon_{ijm} q_m) + \epsilon_{ijl} (\pm i \epsilon_{ikm} r_m)] , \quad (5.4)$$

resulting in the vertex factor in fig. 5-2d,

$$-i g f^{abc} [(r - q)_i \delta_{jk} + (q - p)_k \delta_{ij} + (p - r)_j \delta_{ki}] , \quad (5.5)$$

which can be recognized as the usual three-point vertex factor of QCD₄ in the temporal gauge. The ∂_ν part in the Θ -factor does not contribute to the vertex factor (5.5), because the permutations of it sum to a total derivative, which is identically zero since

$$\Delta_{ij}^{AA}(p, t_1, t) = \Delta_{ij}^{AA}(p, t_2, t) = 0 . \quad (5.6)$$

Next we consider the π - π propagators. Since we are interested in only calculating expectation values of the physical A -field, π - π propagators can occur only as internal lines in first order formalism diagrams. The identity (5.3), involving the π - π propagator, can be expressed in terms of diagrams shown in fig. 5-3. The four-point interaction in fig. 5-3b arises from the $-\delta_{ij} \delta(t - t')$ term in identity (5.3). Therefore, its vertex factor is obtained by a simple contraction of two first order formalism vertices. That is,

$$\begin{aligned} & (-g \epsilon_{ijm} f^{abe} g \epsilon_{klm} f^{cde}) + (\text{two other permutations}) \\ & = -g^2 [(\delta_{ik} \delta_{jl} - \delta_{il} \delta_{jk}) f^{abe} f^{cde} + (\text{two other permutations})] , \end{aligned} \quad (5.7)$$

which is, in fact, the usual four-point vertex of QCD₄.

As shown in fig. 5-3, π - π internal lines are equivalent to the usual QCD₄ four-point interactions of A -fields and extra three-point interactions involving Θ -factors. Diagrams that contain the latter can be summed with the other diagrams of the same order in perturbation theory. The resulting sum consists of diagrams containing only A - A propagators with Θ -factors inserted in all three possible positions around every three-point vertex. As illustrated in fig. 5-2, these Θ -factors can be absorbed into the new three-point vertex (5.5). Thus, diagrams in the first order formulation are equivalent to diagrams that contain only A - A propagators with the usual temporal gauge QCD₄ three and four-point interactions given by eq. (5.5) and eq. (5.7).

To clarify these rules, we give the example of the reorganization of the order g^2 two-point function. As discussed in the first part of this section, the process of converting first order formulation diagrams into finite-time

Feynman diagrams consists of two steps. The first step, illustrated in fig. 5-4, consists of replacing the π - A propagator (4.1) and the π - π propagator (4.2) with A - A propagators (3.7) and Θ -factors (5.2). From the π - π propagator there is an additional δ -function contribution that generates the four-point interaction. The second step, illustrated in fig. 5-5, consists of absorbing the Θ -factors into the three-point vertices, in order to generate the usual QCD₄ vertex factor (5.5).

As previously claimed the diagrammatic rules described in this section are precisely the finite-time Feynman rules of QCD₄ in the temporal gauge. We can check this as follows. In the standard temporal gauge formulation of QCD₄, the generating functional is given by:

$$Z[J] = N \exp \left[\int_{t_1}^{t_2} dt \int d^3x \left(g f^{abc} \frac{\delta}{\delta J_i^a} \frac{\delta}{\delta J_j^b} \partial_i \frac{\delta}{\delta J_j^c} - \frac{1}{4} g^2 f^{abe} f^{cde} \frac{\delta}{\delta J_i^a} \frac{\delta}{\delta J_j^b} \frac{\delta}{\delta J_i^c} \frac{\delta}{\delta J_j^d} \right) \right] Z_0[J], \quad (5.8)$$

where the free generating functional is

$$Z_0[J] = N' \int_{A_i^a(t_1)=0}^{A_i^a(t_2)=0} D A_i^a \exp \left[\int_{t_1}^{t_2} dt \int d^3x \left(\frac{1}{2} A_i^a [(\partial_i^2 + \nabla^2) \delta_{ij} - \partial_i \partial_j] A_j^a + J_i^a A_i^a \right) \right]. \quad (5.9)$$

From the form of the interaction it is clear that eq. (5.8) generates a three- and four-point vertex with the same factors (5.5, 5.7) as arrived at through the first order formalism. $Z_0[J]$ is the finite T free generating functional. Due to the nontrivial nature of the finite T boundary conditions, the zeroth order map was employed as a simple technical tool for the computation of $Z_0[J]$, though other methods can be used [7]. The free gluon propagator, in $Z_0[J]$, turns out to be just the Δ_{ij}^{AA} propagator (3.5a) that we have been using. Therefore, as promised, the first order diagrams are shown to be completely equivalent to the Feynman diagrams in the standard formulation of QCD₄. These finite T Feynman rules are given in fig. 5-6.

Several remarks are in order. First, the form of the finite T gluon propagator shows that the infrared problem of the usual temporal gauge infinite T formulation does not arise as long as one is working at finite T . In fact, this behavior is similar to what happens in the five-dimensional gluon propagator of Parisi and Wu's stochastic quantization [6]. When t_1 and t_2 are respec-

tively taken to negative and positive infinity, the transverse part equilibrates,

$$\frac{1}{p \sinh[pT]} [\theta(t' - t) \sinh[(t - t_1)p] \sinh[(t_2 - t')p] + (t \leftrightarrow t')] \xrightarrow[t_1 \rightarrow -\infty]{t_2 \rightarrow \infty} \frac{e^{-|t-t'|p}}{2p}, \quad (5.10)$$

while the longitudinal part diverges as $-t_1$ or t_2 ,

$$\frac{1}{T} [\theta(t' - t) (t - t_1)(t_2 - t') + (t \leftrightarrow t')] \xrightarrow[t_1 \rightarrow -\infty]{t_2 \rightarrow \infty} -t_1 + \min[t, t'] \\ \xrightarrow[t_1 \rightarrow -\infty]{t_2 \rightarrow \infty} t_2 - \max[t, t']. \quad (5.11)$$

As with Parisi and Wu's stochastic quantization it is not necessary to fix the residual gauge invariance of the maps, or equivalently the path integral formulation. The divergence in the longitudinal part arises for the same reason as in Parisi and Wu's case, and can be interpreted as a random walk in the gauge parameter space [6].

Second, as a final check, we made contact with the usual infinite T formulation of QCD₄ by Fourier transforming the time variables of Δ_{ij}^{AA} in the infinite T limit. The temporal Fourier transform of its transverse part (5.10) is

$$\int_{-\infty}^{\infty} dt e^{-i\omega t} \int_{-\infty}^{\infty} dt' e^{-i\omega' t'} \frac{e^{-|t-t'|p}}{2p} = 2\pi\delta(\omega + \omega') \frac{1}{\omega^2 + p^2}. \quad (5.12)$$

The longitudinal contribution is given by

$$\int_{-\frac{T}{2}}^{\frac{T}{2}} dt e^{-i\omega t} \int_{-\frac{T}{2}}^{\frac{T}{2}} dt' e^{-i\omega' t'} \left[\frac{1}{T} \theta(t' - t) (t + T/2)(T/2 - t') + (t \leftrightarrow t') \right] \\ = -\frac{1}{\omega\omega'} \frac{\sin[(\omega + \omega')T/2]}{(\omega + \omega')/2} + O(T^{-1}) \\ \xrightarrow{T \rightarrow \infty} 2\pi\delta(\omega + \omega') \frac{1}{\omega^2}, \quad (5.13)$$

where we have set $t_1 = -T/2$ and $t_2 = T/2$ for simplicity. Summing up these two limits, one obtains the infinite T limit of the (ω, \vec{p}) space gluon propagator,

$$\Delta_{ij}^{QCD}(\omega, p) = \frac{1}{\omega^2} \hat{L}_{ij} + \frac{1}{\omega^2 + p^2} \hat{T}_{ij}, \quad (5.14)$$

recovering the standard temporal gauge result of QCD₄.

Third, we restate our observation concerning the superficial quadratic divergences in QCD₄. All through the computation we kept track of the one-loop superficial quadratic divergence, and it can be traced back to the higher order contributions of the final state constraint. This observation is made possible only through the map viewpoint. Once the map diagrams are reorganized, the intuition of this fact is lost because the t_2 vertices are absorbed

into the definition of the new propagators. The usual Feynman diagram formulation is simpler in the sense that there are fewer diagrams. However, for the purpose of understanding the connection of the final state constraint to the superficial quadratic divergence, the Feynman formulation is not as helpful as the first order formulation, because both the constraint and basic diagrams are combined. In the first order formulation the quadratically divergent diagram comes purely from map diagrams that include constraint propagators.

So far, we have shown the connection between the superficial quadratic divergence and a particular choice of final and initial states; namely, $I = F = 0$. In the next section we will check that the divergence persists for any choice of I and F .

6. Nonzero initial and final states

In all of the preceding calculations, the initial and final field configurations were assumed to be zero. As can be expected, inclusion of the nonzero initial and final configurations give rise to new Feynman diagrams at finite T . One usually expects, in field theory, that in the infinite T limit, any expectation value is independent of the choice of initial and final states. However, this is not strictly true in gauge theories, because there does not exist a mass gap without gauge fixing. As we shall see here, large T does not wipe out dependence on the longitudinal parts of I and F , which generates new "boundary diagrams" for all n -point correlation functions, even at large T .

Following the same procedure as in the case of zero initial and final states, the corrections to the map diagrams (section 3) can be found. These additional diagrams can be rearranged to give extra contributions to the finite-time Feynman diagrams. Alternatively, the finite-time QCD₄ generating functional including the $I, F \neq 0$ contributions can be evaluated. As for the generating functional with $I, F = 0$ (5.8), the interacting part of the generating functional with $I, F \neq 0$ can be pulled out of the functional integral. The free generating functional, including the nontrivial boundary conditions, can be evaluated with the aid of the map.

$$Z_0^S[J] = \exp \left[\frac{1}{2} \int_{t_1}^{t_2} dt dt' \int d^3x d^3x' J_i^a(\vec{x}, t) \Delta_{ij}^{AA}(\vec{x}, t; \vec{x}', t') J_j^a(\vec{x}', t') + \int_{t_1}^{t_2} dt \int d^3x J_i^a(\vec{x}, t) S_i^a(\vec{x}, t) \right], \quad (6.1)$$

where the boundary term, S_i^a , is related to the initial and final states by the equation

$$S_i^a(\vec{x}, t) = \left[\frac{t-t_1}{T} \hat{L}_{ij} + \frac{\sinh[(t-t_1)\sqrt{-\nabla^2}]}{\sinh[T\sqrt{-\nabla^2}]} \hat{T}_{ij} \right] F_j^a(\vec{x}) + \left[\frac{t_2-t}{T} \hat{L}_{ij} + \frac{\sinh[(t_2-t)\sqrt{-\nabla^2}]}{\sinh[T\sqrt{-\nabla^2}]} \hat{T}_{ij} \right] I_j^a(\vec{x}). \quad (6.2)$$

Because of the boundary term (6.2), there are new contributions to every n -point correlation function. For example, the expectation value of the A -field, which is zero in the case of vanishing boundary terms, becomes

$$\langle A_i^a(\vec{x}, t) \rangle = S_i^a(\vec{x}, t) + O(g). \quad (6.3)$$

The general diagrammatic rules in (t, \vec{p}) space for calculating the new contributions to the n -point correlation function,

$$\int d^3x_1 \cdots d^3x_n e^{i\vec{p}_1 \cdot \vec{x}_1 + \cdots + i\vec{p}_n \cdot \vec{x}_n} \langle A_{i_1}^{a_1}(\vec{x}_1, \tau_1) \cdots A_{i_n}^{a_n}(\vec{x}_n, \tau_n) \rangle, \quad (6.4)$$

are as follows. The boundary insertion $\tilde{S}_i^a(\vec{p}, t)$, which is the spatial Fourier transform of $S_i^a(\vec{x}, t)$, is represented by a wavy line with a small circle attached, as shown in fig. 6-1. By inspecting the free generating functional (6.1) and the interaction of eq. (5.8), one sees that an $I, F \neq 0$ insertion can be connected to other $I, F \neq 0$ insertions or gluon propagators through the usual three- and four-point vertices of QCD₄. These new vertices are depicted in fig. 6-2.

Since the $I, F \neq 0$ terms in the free generating functional do not affect the interactions, the vertex factors for the nonzero I and F vertices in fig. 6-2 are just the usual three- and four-point vertex factors of QCD₄. As in the case of $I, F = 0$, spatial momenta are conserved at all vertices, all intermediate times are integrated from t_1 to t_2 and all internal momenta are integrated. Combinatoric factors for identical gluons, as well as combinatoric factors for $I, F \neq 0$ insertions should also be included as usual. As an example, the order g contribution to the two-point function is given in fig. 6-3, which is equivalent to the equation,

$$\begin{aligned} & \int d^3x \int d^3x' e^{-i\vec{p} \cdot \vec{x}} e^{-i\vec{q} \cdot \vec{x}'} \langle A_i^a(\vec{x}, t) A_j^b(\vec{x}', t') \rangle^{(1)} \\ &= -ig f^{abc} [(r-q)_i \delta_{jk} + (q-p)_k \delta_{ij} + (p-r)_j \delta_{ki}] \\ & \quad \times \int_{t_1}^{t_2} dr \Delta_{i\vec{r}}^{AA}(p, t, r) \Delta_{j\vec{r}}^{AA}(q, t', r) S_k^c(r, r), \end{aligned} \quad (6.5)$$

where $r = -(p+q)$. To further illustrate the procedure, the order g^2 $I, F \neq 0$ contributions to the two-point functions are depicted in fig. 6-4. These diagrams are tree diagrams, which are finite, and therefore, can not affect the order g^2 quadratic divergences of the two point function.

These $I, F \neq 0$ contributions to the n -point functions do not conserve spatial momentum, because initial and final configurations other than constants break spatial translation invariance. Although spatial momentum is conserved at each vertex, the $I, F \neq 0$ insertions act as sources or sinks of momentum. As a result the sum of all external momenta does not necessarily vanish. Moreover, the definition (6.4) is different from the usual definition of the momentum space n -point function—in which the overall momentum δ -function is factored out. The n -point function generated by the diagrammatic rules of the last section is of the latter type. To consistently add these new $I, F \neq 0$ contributions to the $I, F = 0$ contributions of the last section, extra overall momentum conserving δ -functions, $(2\pi)^3 \delta^3(\sum p)$, should be multiplied onto the diagrams of the last section.

In the infinite T limit, the transverse part of the boundary term, S_i^a , damps out and only the longitudinal part persists. This fact is intimately connected to the residual spatial gauge invariance of the theory. As with Parisi and Wu's stochastic quantization, one can expect that if one calculates only gauge invariant quantities, the boundary term will not affect the result [6]. In fact, what is usually done in QCD₄ is to set these contributions to zero by implicitly choosing the longitudinal part of I and F to vanish. Alternatively, as emphasized by Claudson and Halpern, the amplitudes satisfy Gauss' law when smeared over a gauge invariant initial or final state, so with this prescription, the large T limits should be independent of I and F .

7. Conclusions and comments

The major points presented in this paper were:

- 1) The explicit reorganization of the Claudson-Halpern QCD₄ map diagrams into temporal gauge finite-time Feynman diagrams.
- 2) Three finite-time, infrared finite, perturbation expansions of QCD₄ are discussed. In one of these formulations, the first order formulation, the one loop superficial quadratic divergences are found in a single diagram.
- 3) The superficial quadratic divergences of QCD₄, at least in the temporal gauge, are related to a choice of any particular final state in the Feynman path integral. This can only be seen in the map formulation.

4) By working at finite-time, we have seen that there is no need to fix the residual spatial gauge invariance in the maps (or equivalently the path integral formulation in the temporal gauge). The result is a random walk in the gauge parameter space, exactly as in Parisi and Wu's fifth-time stochastic quantization. The "miracle" of not having to gauge fix is not particular to the (artificial) fifth-time stochastic quantization.

5) In the infinite-time limit, the longitudinal part of boundary terms persist. These terms are not expected to affect the gauge invariant quantities, in analogy with Parisi and Wu's stochastic quantization. The phenomenon of longitudinal memory is common to any system with longitudinal zero modes.

6) The stochastic regularization proposed by Claudson and Halpern [1] fails because their scheme does not regularize the quadratically divergent constraint diagrams.

Less formal studies of the maps will require a regularization scheme.

8. Acknowledgements

The authors would like to thank Prof. M.B. Halpern for many helpful discussions and advice. This work was supported by the Director, Office of Energy Research, Office of High Energy and Nuclear Physics, Division of High Energy Physics of the US Department of Energy under contract DE-AC03-76SF00098.

References

- [1] M. Claudson and M.B.Halpern, "Nicolai maps for QCD_4 ",
LBL-18355 (1984) (accepted for publication in Phys. Letts.)
- [2] M.Claudson and M.B. Halpern, "Nicolai maps and fermion sectors",
UCB-PTH-84/28 (1984)
- [3] H. Nicolai, Phys. Lett. 89B (1980) 341;
H. Nicolai, Phys. Lett. 117B (1982) 408
- [4] N.G. van Kampen, Stochastic processes in chemistry and physics
(North-Holland, Amsterdam, 1981)
- [5] H. Loos, Phys. Rev. 188 (1969) 2342;
J.P. Greensite, Nucl. Phys. B158 (1979) 469
- [6] G. Parisi and Wu Yong-Shi, Sci. Sin. 24 (1981) 483
- [7] R.P. Feynman and A.R. Hibbs, Quantum mechanics and path integrals
(McGraw-Hill, New York, 1965)

Figure Captions

- Figure 2-1 QCD₄ as a brownian motion: Only those paths that end at F are accepted.
- Figure 2-2 Diagrammatic representation of the iterative solution to the maps.
- Figure 2-3 Two-point "pure map" diagrams ignoring the final state constraint.
- Figure 3-1 Vertex factors in map formulation.
- Figure 3-2 Map diagrams for the two-point function.
- Figure 4-1 First order formulation propagators as combinations of map propagators.
- Figure 4-2 Three-point couplings in the first order formulation.
- Figure 4-3 First order formulation diagrams for the order g^2 two-point function.
- Figure 4-4 Quadratic divergence in map and first order formulation.
- Figure 5-1 Decomposition of π - A propagator into an A - A propagator and Θ -factor.
- Figure 5-2 Decomposition of first order formulation vertices into QCD₄ three-point vertices.
- Figure 5-3 Decomposition of internal π - π propagator into A - A propagator. The diagrams in (a) represent part of an arbitrary first order formalism diagram.
- Figure 5-4 The first step in conversion to usual Feynman diagrams consists of replacing π - A and π - π propagators with A - A propagators. The π - π propagator produces an additional δ -function contribution that generates the four-point interaction. Diagram (a) includes an implicit combinatoric factor of $1/2$.
- Figure 5-5 The second step consists of absorbing the Θ -factors shown in fig. 5-4 into three-point vertices.
- Figure 5-6 Temporal gauge Feynman rules for all T in (t, \vec{p}) space. Integration over intermediate times from t_1 to t_2 is implied.
- Figure 6-1 Diagrammatic representation of the $I, F \neq 0$ insertions.
- Figure 6-2 $I, F \neq 0$ vertices.
- Figure 6-3 Order g contribution to the two-point function.
- Figure 6-4 Order g^2 $I, F \neq 0$ contribution to the two-point function.

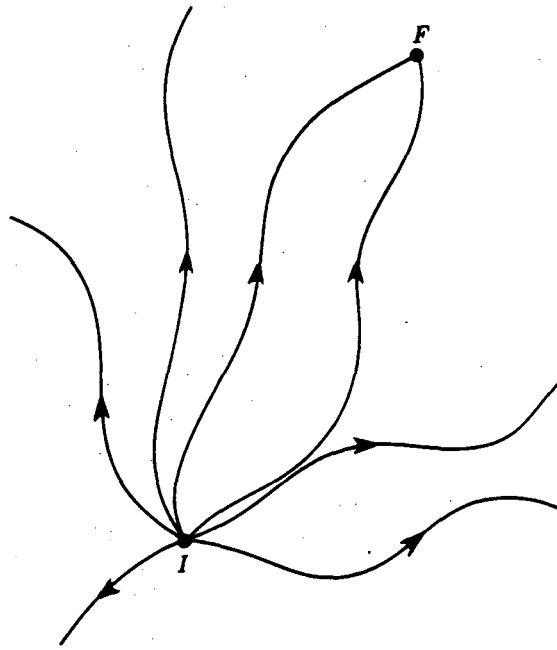


Figure 2-1

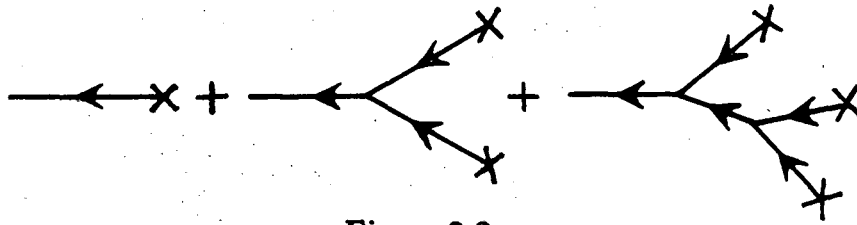


Figure 2-2

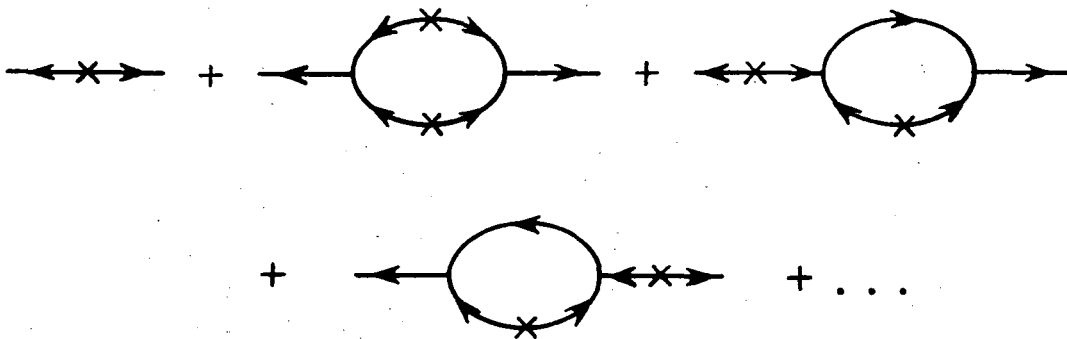
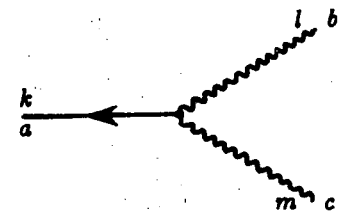
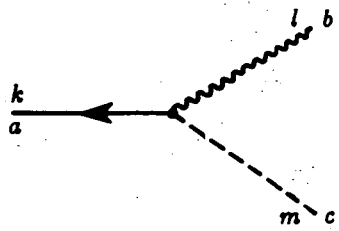


Figure 2-3

(a)  $= -\delta^{ab}$

(b)  $= i\delta^{ab}$

(c)  $= \pm g f^{abc} \epsilon_{klm}$

(d)  $= \pm g f^{abc} \epsilon_{klm}$

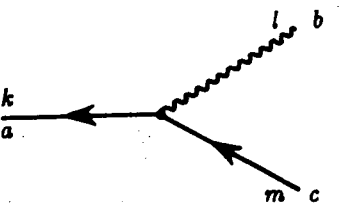
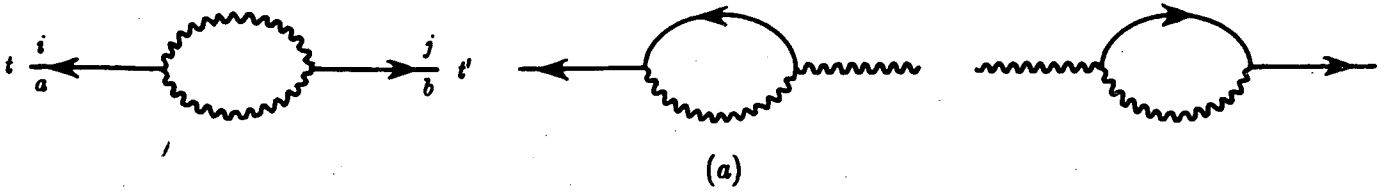
(e)  $= \pm g f^{abc} \epsilon_{klm}$

Figure 3-1

Basic diagrams:



Constraint diagrams:

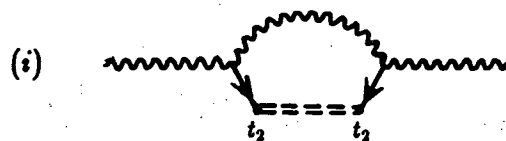
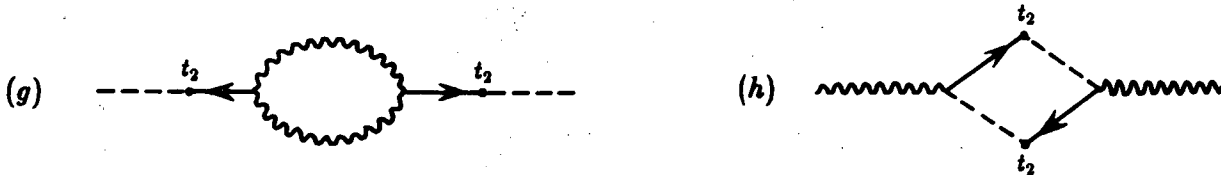
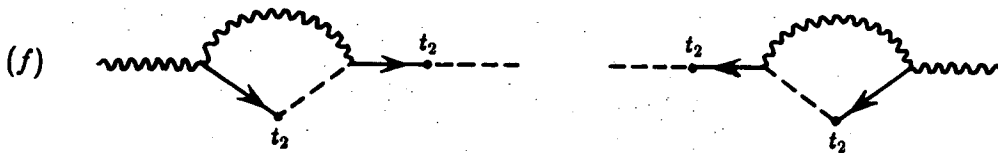
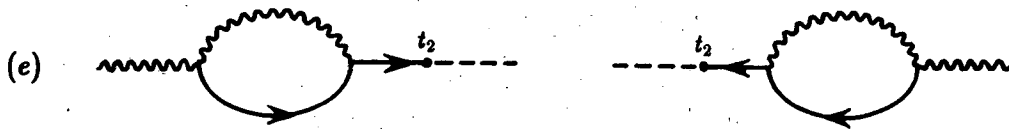
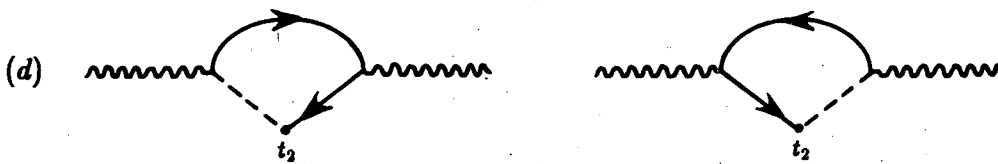
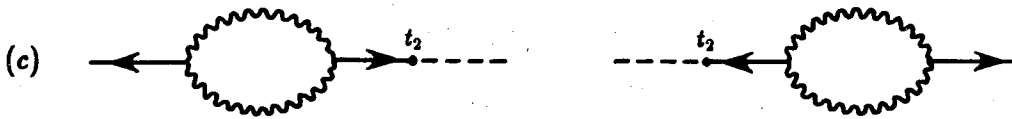
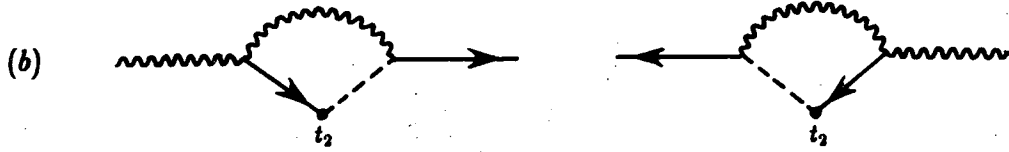


Figure 3-2

$$\begin{aligned}
 (a) \quad \delta^{ab} \Delta_{ij}^{\pi A \pm}(p, t', t) &\equiv t' \overset{a}{i} \overset{\pi}{\rightsquigarrow} \overset{A}{\rightsquigarrow} \overset{b}{j} t \\
 &= t' \overset{a}{i} \overset{\rightarrow}{\rightsquigarrow} \overset{b}{j} t + t' \overset{a}{i} \overset{\rightarrow}{\rightsquigarrow} \overset{t_2}{k} \overset{\dashrightarrow}{\rightsquigarrow} \overset{b}{j} t
 \end{aligned}$$

$$\begin{aligned}
 (b) \quad \delta^{ab} \Delta_{ij}^{\pi \pi \pm}(p, t', t) &\equiv t' \overset{a}{i} \overset{\pi}{\rightsquigarrow} \overset{\pi}{\rightsquigarrow} \overset{b}{j} t \\
 &= t' \overset{a}{i} \overset{\rightarrow}{\rightsquigarrow} \overset{t_2}{k} \overset{=} \overset{t_2}{l} \overset{\leftarrow}{\rightsquigarrow} \overset{b}{j} t
 \end{aligned}$$

Figure 4-1

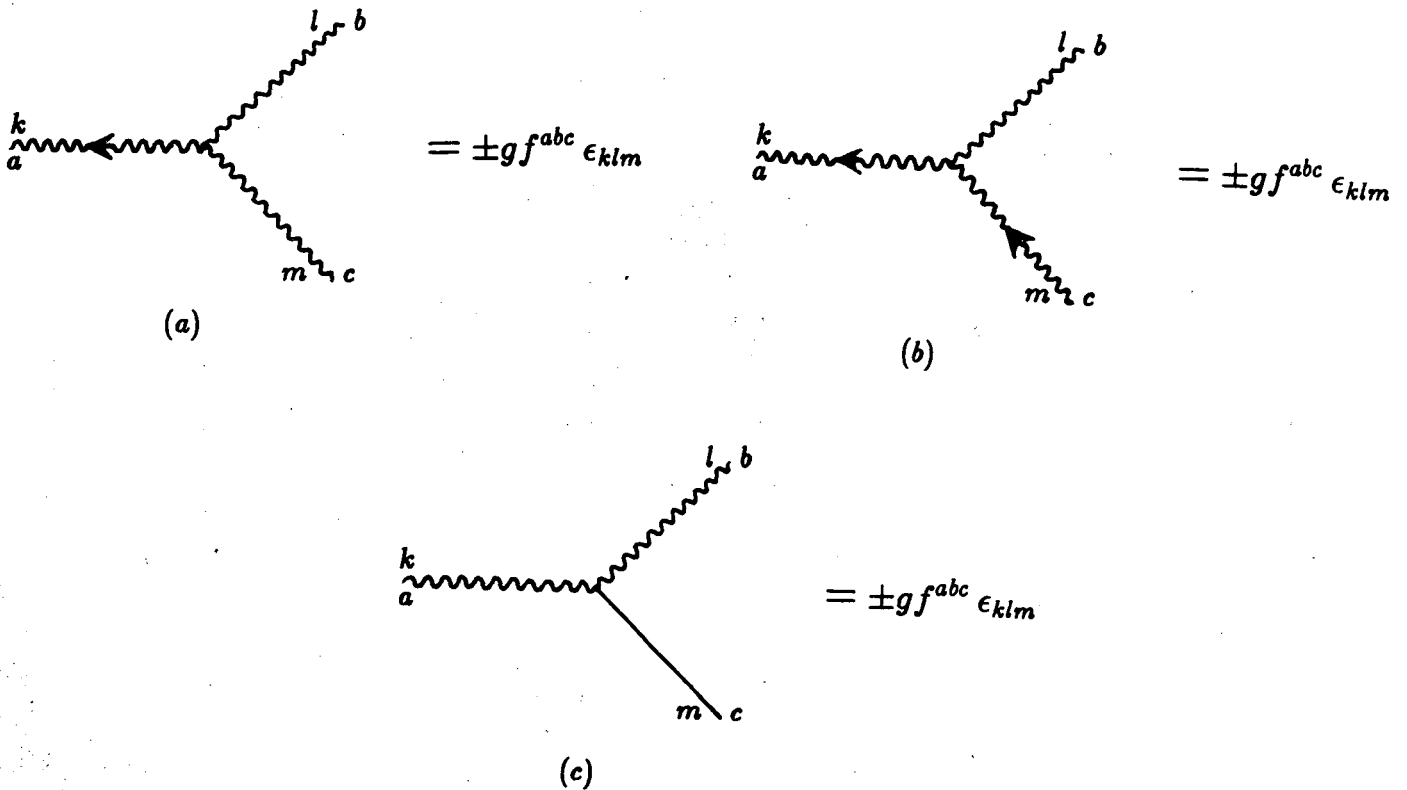


Figure 4-2

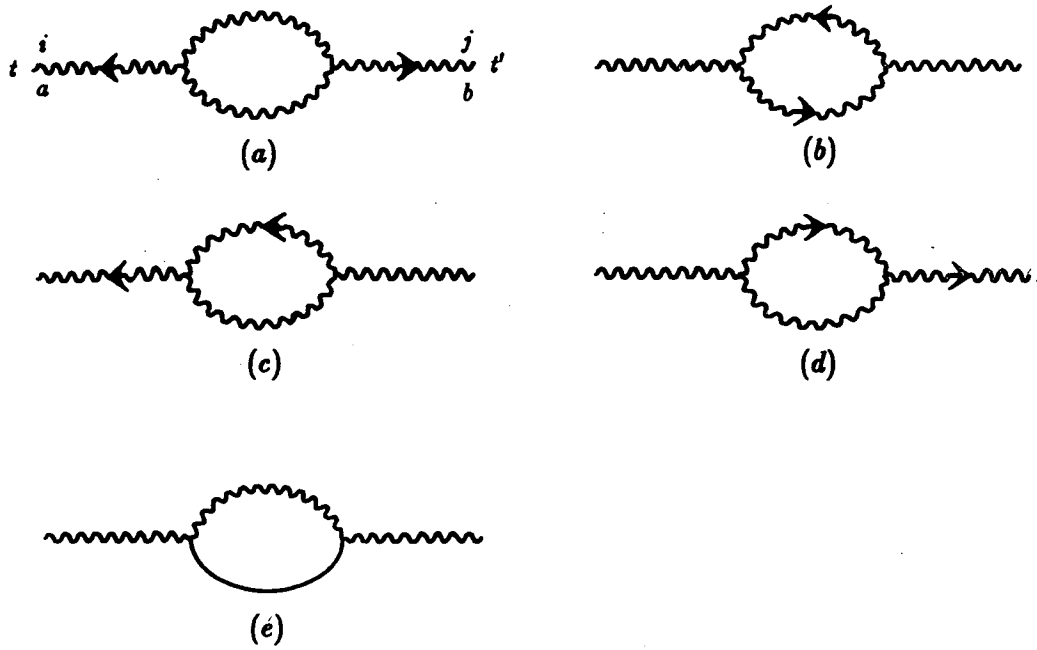


Figure 4-3

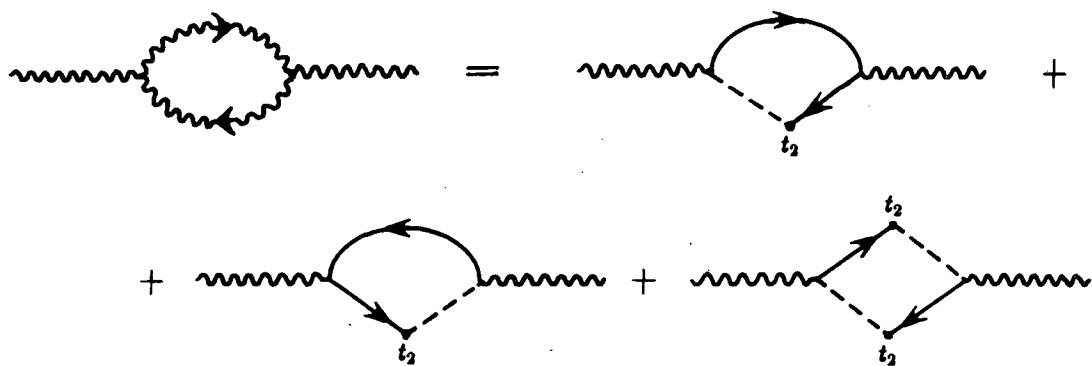


Figure 4-4

$$\begin{aligned} \frac{t'}{i} \rightarrow \bigcirc_k^t &= \Theta_{ik}^\pm(p, t', t) \\ t' \xrightarrow{\pi} \xrightarrow{A} j \xrightarrow{t} &= t' \rightarrow \bigcirc_k \xrightarrow{A} j \xrightarrow{t} \end{aligned}$$

Figure 5-1

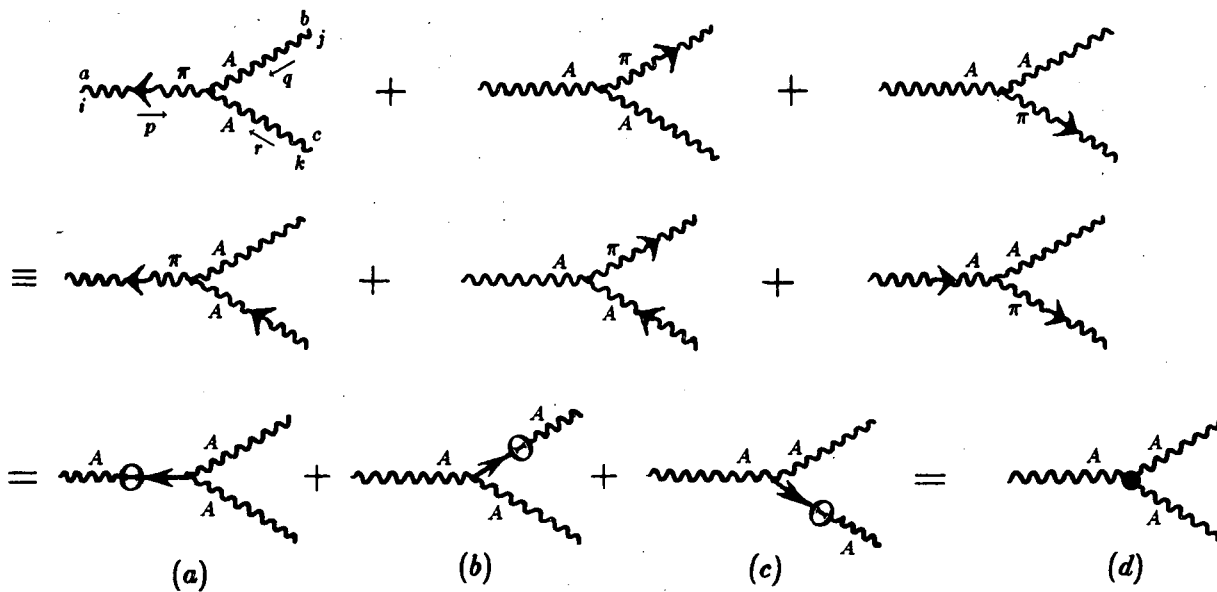


Figure 5-2

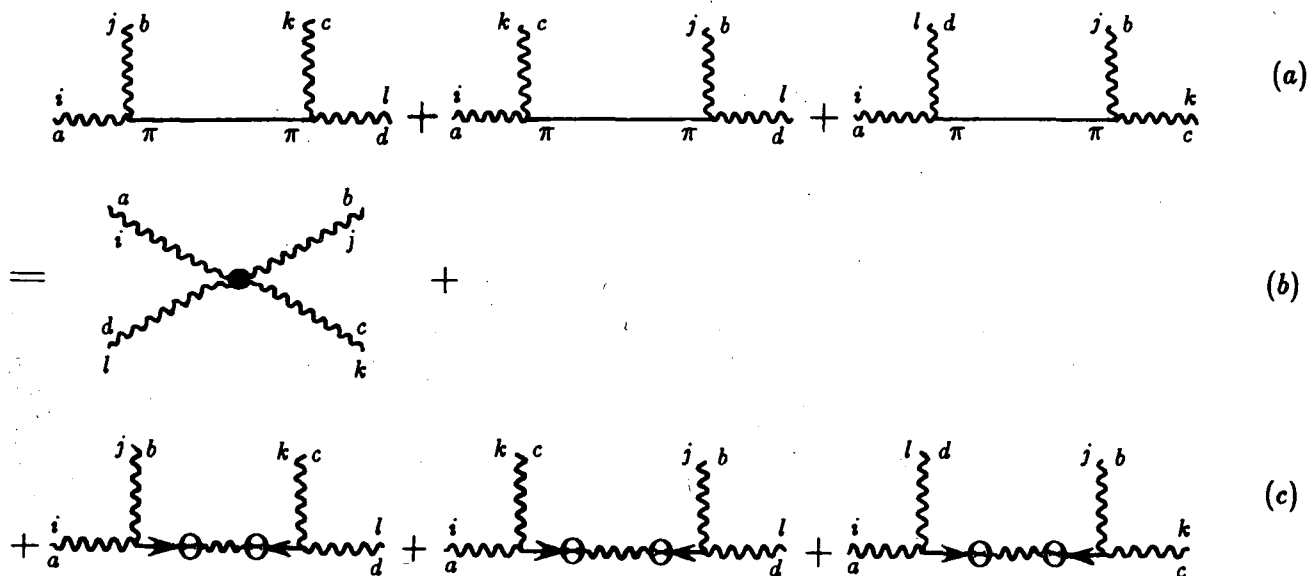
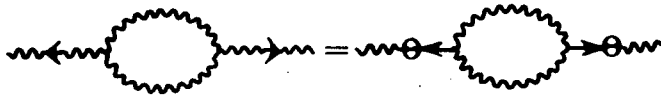
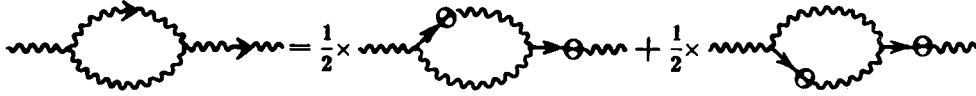


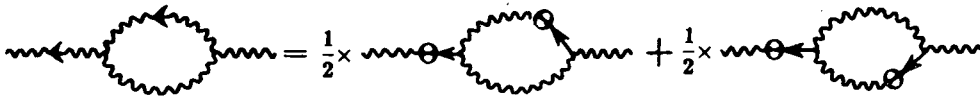
Figure 5-3



(a)



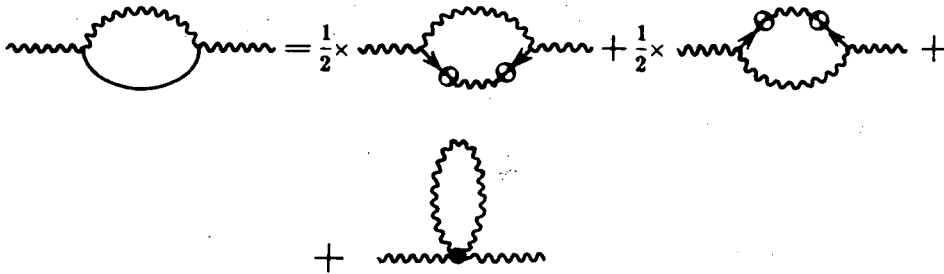
(b)



(c)



(d)



(e)

Figure 5-4

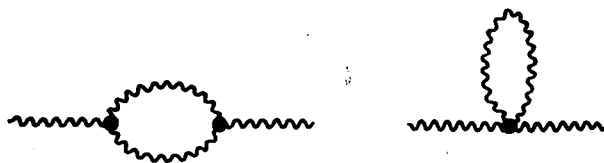


Figure 5-5
28

Propagators:

$$t \begin{array}{c} a \\ \text{~~~~~} \\ i \end{array} \begin{array}{c} \text{~~~~~} \\ b \\ j \end{array} t' = \delta^{ab} \Delta_{ij}^{AA}(p, t, t') \quad [\text{c.f. (3.7)}]$$

Vertices:

$$\begin{array}{c} b \\ \text{~~~~~} \\ j \end{array} \begin{array}{c} a \\ \text{~~~~~} \\ i \end{array} \begin{array}{c} \text{~~~~~} \\ c \\ k \end{array} \begin{array}{c} \text{~~~~~} \\ r \end{array} = -ig f^{abc} [(\mathbf{r} - \mathbf{q})_i \delta_{jk} + (\mathbf{q} - \mathbf{p})_k \delta_{ij} + (\mathbf{p} - \mathbf{r})_j \delta_{ki}]$$

$$\begin{array}{c} a \\ \text{~~~~~} \\ i \end{array} \begin{array}{c} \text{~~~~~} \\ j \\ b \end{array} \begin{array}{c} \text{~~~~~} \\ k \\ c \end{array} \begin{array}{c} \text{~~~~~} \\ d \end{array} = -g^2 [(\delta_{ik} \delta_{jl} - \delta_{il} \delta_{jk}) f^{abe} f^{cde} \\ + (\delta_{ik} \delta_{jl} - \delta_{ij} \delta_{lk}) f^{cbe} f^{ade} \\ + (\delta_{lk} \delta_{ij} - \delta_{jk} \delta_{il}) f^{dbe} f^{cae}]$$

Figure 5-6

$$t \begin{array}{c} \overleftarrow{p} \\ \text{wavy line} \\ a \\ i \end{array} \bigcirc = \tilde{S}_i^a(p, t)$$

Figure 6-1

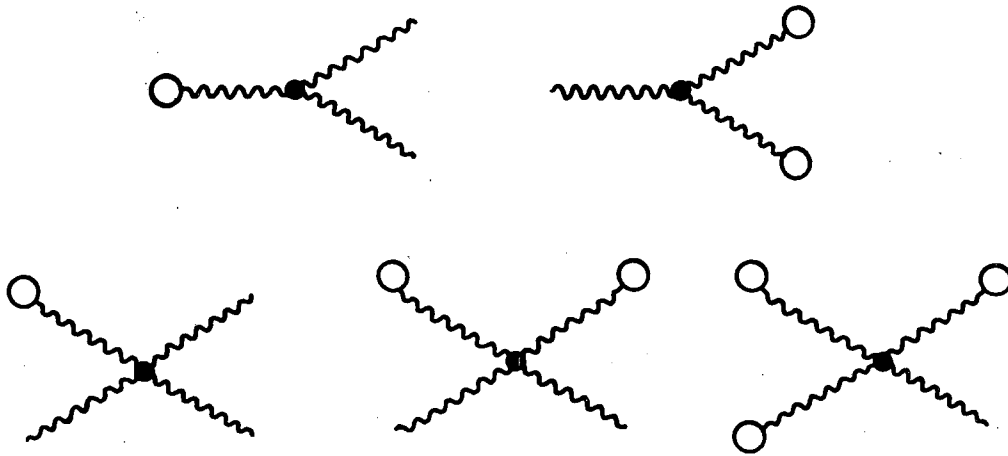


Figure 6-2

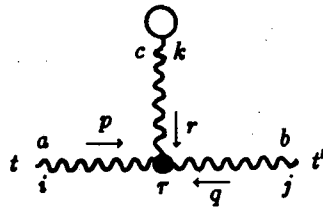


Figure 6-3

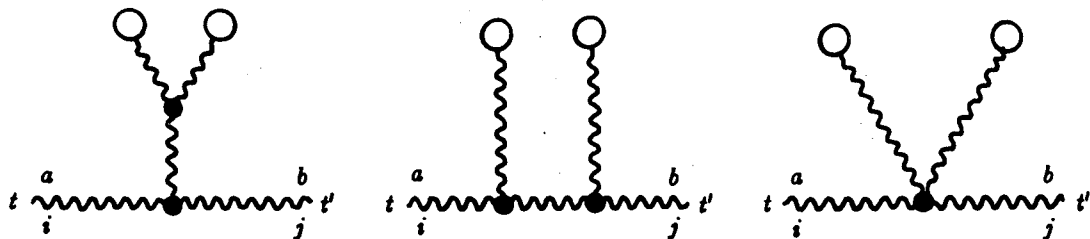


Figure 6-4

This report was done with support from the Department of Energy. Any conclusions or opinions expressed in this report represent solely those of the author(s) and not necessarily those of The Regents of the University of California, the Lawrence Berkeley Laboratory or the Department of Energy.

Reference to a company or product name does not imply approval or recommendation of the product by the University of California or the U.S. Department of Energy to the exclusion of others that may be suitable.

TECHNICAL INFORMATION DEPARTMENT
LAWRENCE BERKELEY LABORATORY
UNIVERSITY OF CALIFORNIA
BERKELEY, CALIFORNIA 94720